DEUTSCHES ELEKTRONEN – SYNCHROTRON DESY

DESY SR 87-07
July 1987

CONTRIBUTIONS OF THE NIKOS GROUP TO THE 1st FRASCATI MEETING ON SYNCHROTRON RADIATION APPLICATIONS TO DIGITAL SUBTRACTION ANGIOGRAPHY

by

W.-R. Dix

Deutsches Elektronen-Synchrotron DESY, Hamburg

W. Graeff, J. Heuer

Hamburger Synchrotronstrahlungslabor HASYLAB at DESY

K. Engelke, C.-C. Glüer, H. Jabs, C. P. Höppner

II. Inst. f. Experimentalphysik, Universität Hamburg

W. Kupper, P. Steiner, W. Bleifeld

Kardiologische Abt. der II. Medizinischen Klinik, Universitäts-Krankenhaus Eppendorf, Hamburg

K. H. Höhne, K. H. Stellmaschek

Inst. f. Mathematik u. Datenverarbeitung in der Medizin, Universitäts-Krankenhaus Eppendorf, Hamburg

ISSN 0723-7979

NOTKESTRASSE 85 · 2 HAMBURG 52

To be sure that your preprints are promptly included in the
HIGH ENERGY PHYSICS INDEX,
send them to the following address (if possible by air mail):

DESY
Bibliothek
Notkestrasse 85
2 Hamburg 52
Germany

DESY SR 87-07
July 1987

ISSN 0723-7979

Contributions of the NIKOS Group to the 1st Frascati Meeting on Synchrotron Radiation Applications to Digital Subtraction Angiography

W.-R. Dix
Deutsches Elektronen-Synchrotron DESY, Hamburg

W. Graeff J. Heuer
Hamburger Synchrotronstrahlungslabor HASYLAB at DESY, Hamburg

K. Engelke C.-C. Glüer[1] H. Jabs
C.P. Höppner[2]
II. Inst. für Experimentalphysik, Universität Hamburg. Hamburg

W. Kupper P.Steiner
W. Bleifeld
Kardiologische Abt. der II. Medizinischen Klinik,
Universitäts-Krankenhaus Eppendorf, Hamburg

K.H. Höhne K.H. Stellmaschek
Inst. für Mathematik und Datenverarbeitung in der Medizin,
Universitäts-Krankenhaus Eppendorf, Hamburg

6-8 May 1987

to be published in: Conference Proceedings Series ed. by
Società Italiana di Fisica

[1]present address: University of California, San Francisco
[2]present address: Siemens, Erlangen

Contents

Chapter 1

An Overview of Different Technical Approaches to SYRDA

1.1 Introduction

The intravenous application of iodine contrast material results in an iodine concentration of $10mg/ml$ in the coronary arteries under the assumption that $10ml$ Urografin ($370mg/ml$ iodine) is injected within $1s$ into a brachial vein. In a conventional transmission radiograph such a low concentration in a $1mm$ thick vessel would give a 1.2% signal, only ($50keV$ photons assumed), covered by much stronger tissue and bone contrast.

Intravenous angiography hence requires an iodine selective imaging method. In the following different technical aspects of such a method will be discussed.

1.2 Dichromography or Fluorescence?

On a first glance it looks very promising to excite the iodine atoms in the contrast material by a rapidly scanning pencil beam to detect the **fluorescence** signal (I Kα and Kβ lines), similarly for instance to EXAFS measurements in highly diluted samples. We investigated this possibility by Monte Carlo simulation of the interaction of such a pencil beam with a $20cm$ thick soft tissue cylinder and verified the calculations experimentally with a lucite phantom /1/.

As a result it turned out that the fluorescence signal suffers from a strong background of Compton scattered radiation which cannot be suppressed even by using a solid state detector. A dose comparison of the fluorescence method with the dichromography described further below is for constant signal/noise ratio in favor of the former only up to a vessel $5cm$ below the skin. Similar results are obtained in case of Gadolinium as a contrast material, where the absorption of the photons is smaller but the scatter increases. In addition the strong depth dependence of the signal height gives a very peculiar contrast compared to a transmission radiograph.

For coronary angiography most of the interesting vessels lie deeper than $5cm$ below the skin. Therefore another iodine selective technique, the **dichromography** is obviously more adequate. Here two monochromatic beams bracketing the K-edge of

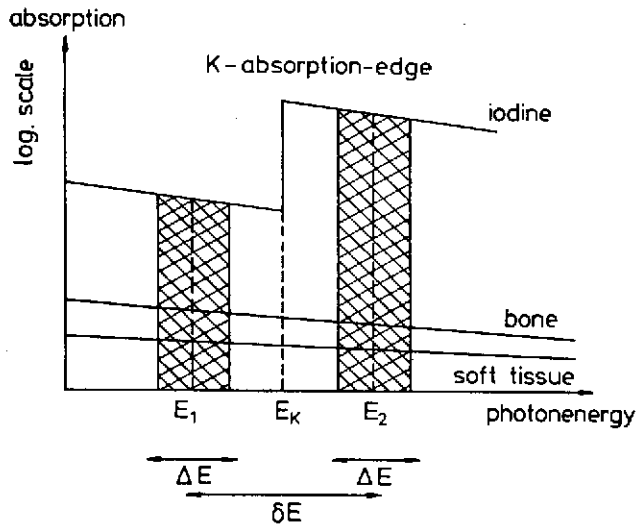

Figure 1.1: Energy dependence of absorption coefficients

iodine (Fig. 1.1) yield two images which are different in iodine containing parts but essentially equal in soft tissue and bone contrast. Hence, the logarithmic subtraction of such image pairs is highly iodine selective. For an energy separation of the beams of $\delta E = 300eV$ a $1mm$ thick vessel shows up as a 3% difference between the two images. The difference signal of soft tissue and bone is by four orders of magnitude smaller. But with increasing δE the sensitivity to normal tissue grows to inacceptable levels. That is the reason why dichromography with conventional sources is by an order of magnitude less sensitive to low iodine concentrations /2/.

During the last years this particular form of DSA was used for coronary angiography at several synchrotron radiation laboratories, namely at Stanford /3/, Novosibirsk /4/, Hamburg /5/ and Tsukuba /6/. They have differences in the technical realisation which will be discussed in the following.

1.3 Imaging Modes

From the medical doctor's point of view **two-dimensional image recording** and, if possible, a cine film, would be most desirable.

But the main draw back of 2D imaging with an area detector is the large amount of scatter especially in the region of the heart. Up to 90% scatter contribution to the directly transmitted signal have been measured /7/ which would considerably reduce the contrast in DSA. Taking provisions against it like antiscatter grids will increase the dose.

A very important point in DSA is the exact **spatial and temporal correspondence** of the volume that contributes to the individual pixels in the two images (Fig. 1.2). Velocity measurements on coronary arteries have shown that for $0.5mm$ spatial resolution corresponding pixels should be recorded within $4 - 5ms$. For 2D imaging two complete frames must be taken within that time posing strong demands on the

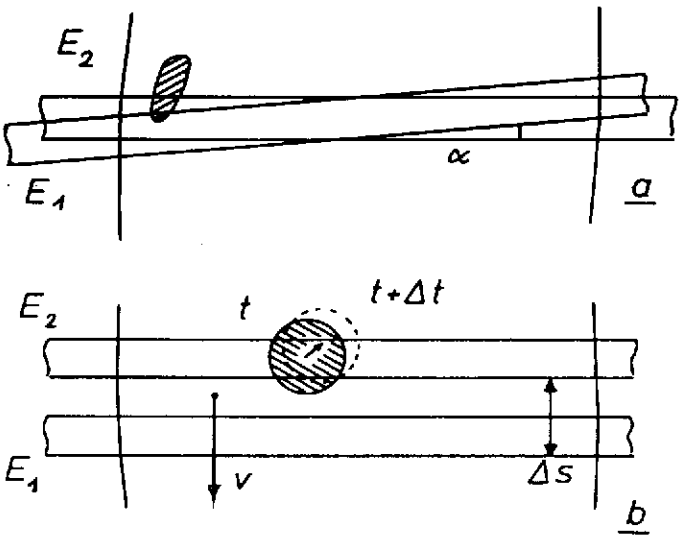

Figure 1.2: Spatial and temporal coherence of the image pairs. (a) Crossing beams, (b) parallel beams with time delay $\Delta t = \Delta s/v$.

source power.

If the two probing beams cross each other within the patient under an angle α, this angle is limited by the spatial resolution and the patient thickness. Typically $0.5mm$ resolution and $20cm$ tissue thickness limits α to about $5 \cdot 10^{-4}$ (80% pixel overlap). With such a limit a $120mm$ high image is separated from the second one after $240m$. Obviously 2D imaging requires a beam which is rapidly switched from one energy to the other.

A line scan mode reduces the scatter contribution to about 1.5% but for practical reasons is much slower. A reasonable scan time should fit into a slow motion phase of the heart, hence should be $200 - 250ms$. Again two different modes can be devised, namely energy switching with recording one line at a time or simultaneous recording of two lines with different energies.

The **one line registration** has the advantage that the characteristics of the detector channels (so-called fixed pattern) are cancelled in the subtracted image but requires a rapid beam switcher like the rotating drum at Stanford. The **two line registration** makes better use of the photon flux, needs no fast moving mechanics, but a special two line detector.

In contrast to the 2D imaging techniques the present line scan schemes require the motion of the patient through the stationary beams. Once the method has been validated against the conventional angiography precision slides will make the beams move for the ease of the patients.

1.4 Monochromators

Before looking at different monochromator configurations we shall estimate the appropriate bandwidth and necessary intensity of the beams.

The **flux** needed in front of the patient can easily be estimated. Aiming at a signal/noise ratio of SNR=3 with a $1mm$ vessel the noise limit is 0.7% in the unsubtracted images (1% in the subtracted image), in other words at least 20,000 photons must be registered per pixel. This leads with a pixel size of $0.5 \times 0.5mm^2$ and $20cm$ of soft tissue to about $5 \cdot 10^7 phot/mm^2$ in front of the patient. The actually needed **intensity** strongly depends on the exposure time of the pixel, the monochromator geometry et cetera. For instance for the NIKOS set-up we estimated $5 \cdot 10^{10} phot/(mm^2 s)$.

It can be shown /8/ that with good approximation the **energy separation** δE of the two mean values E_1 and E_2 of the probing beams but not their **bandwidth** ΔE influences the signal height in the subtracted image. Up to $\delta E = 300eV$ can be tolerated. This leads to a maximal bandwidth $\Delta E \leq 250eV$ safely avoiding the K-edge region, or $\Delta E/E \leq 7 \cdot 10^{-3}$. Such a bandwidth can be achieved by perfect crystal monochromators which consequently are used in all set-ups.

The bandwidth of a perfect crystal reflection can be calculated according to

$$\Delta E/E = \cot \Theta \, (\Delta \Theta + \Delta \Theta_i)$$

with Bragg angle Θ and vertical **beam divergence** $\Delta \Theta$ (including curvature contributions from bent crystals). $\Delta \Theta_i$ denotes the **intrinsic reflection width** which depends on the reflection and the energy. E.g. at $E = 33.17keV$ the Si 111 reflection has a reflection width $\Delta \Theta_i = 8\mu rad$ whereas the full vertical divergence of the synchrotron beam amounts to typically $200\mu rad$. Even with full beam divergence ΔE will be of the order of $100eV$ for a flat crystal which is well below the estimated $250eV$ limit.

With **bent crystals** the increased energy bandwidth might be a problem. Bent crystals can be used either for spreading the beam for full illumination of the heart in 2D imaging (Fig. 1.3a) or for focusing of the full beam height down to the entrance slit height of a line scan system (Fig. 1.3b).

Asymmetrically cut crystals are used to affect the beam dimensions similar to the bent crystals. For 2D imaging the beam can be widened by a factor of about 25 to cover the full heart (Fig. 1.3c). This will reduce the intensity per pixel by a factor of 5 only due to the increased acceptance of the grazing incidence. For line scanning the beam can be compressed by a factor of 10 (Fig. 1.3d), thereby increasing the intensity by a factor of 3 compared to the symmetrically cut crystal.

Using only one crystal reflection per beam certainly has the advantage of being less sensitive to crystal perfection. Even a high quality crystal is affected by heating, keeping in mind that the required flux is only achieved by strong wiggler beams. On the other hand depending on the critical energy of the white synchrotron radiation spectrum contamination of the monochromatic beams by **higher harmonics** (like $66keV$, $99keV$, depending on the crystal reflection) must be considered, which will grow up by beam hardening within the patient and cause contrast losses in the subtracted image. Using only one crystal reflection also leads to an angle α between the probing beams which is twice the difference in Bragg angles of the two reflections. Taking the 80% overlap criterion $0.5mm$ resolution leads to a maximum energy difference of $\delta E = 290eV$. Increasing the resolution with single crystal reflections requires higher monochromaticity.

A double crystal monochromator (Fig. 1.4a) avoids these two problems as the second crystal reflects the beam back to the direction of the incident white beam (hence

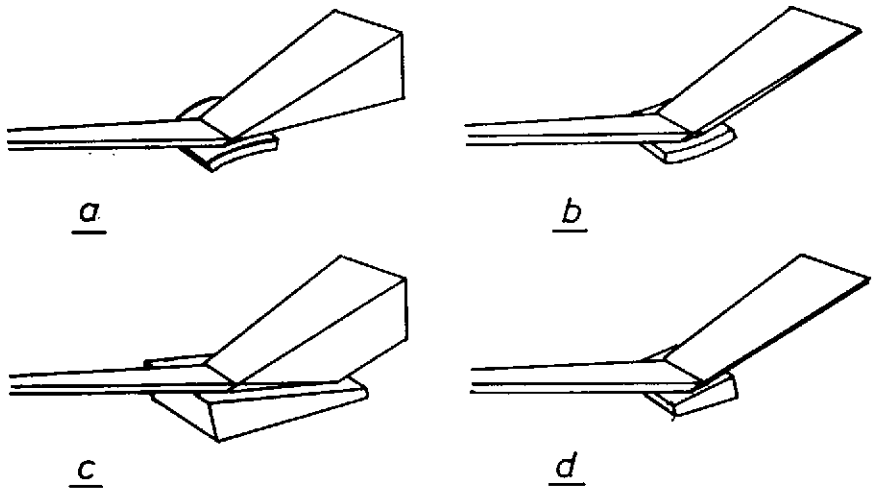

Figure 1.3: Shaping the beam cross section: (a) Bent crystal spreads the beam for 2D imaging, (b) bent crystal focuses the beam for line scanning, (c) and (d) like (a) and (b) but with asymmetric crystals.

$\alpha = 0$), and if properly set, rejects higher harmonics. A successful implementation of such a configuration, however, requires **high quality crystals** at which the crystal bending must be less than $1\mu rad$ over the entire reflecting area.

So-called **Laue crystals** (Fig. 1.4b) the reflecting netplanes of which are perpendicular to the surface, are very promising for our purpose. They can be made very thin so that the full beam height can be used by two successive Laue crystals whereas with usual Bragg crystals the incident beam cross section must be divided among the two beams. In addition Laue crystals, even when flat, focus the beam in vertical direction. A more detailed description is given in chapter 2.

1.5 Detectors

Suitable detectors for angiography have a large dynamic range (about 10^4), a good detective quantum efficiency (≥ 0.5), a time resolution of less than $1ms$ and a spatial resolution of at least $0.5mm$. They may be distinguished by being integrating or single photon counting, having one- or twodimensional position sensitivity, parallel or serial readout, direct or indirect photon conversion etc.

At Stanford a segmented line detector made out of $5mm$ thick Li drifted silicon is used. The X-rays are directly converted into electric charge carriers. The induced photocurrent is simultaneously measured in all channels.

At Novosibirsk a detector based on a large number of NaI scintillator crystals coupled to individual photomultipliers has been tested. This detector is single photon counting up to 1 MHz/channel.

At Hamburg a two line detector has been developed for simultaneous recording of two beams. The X-rays are converted in a phosphor screen to visible light, that is

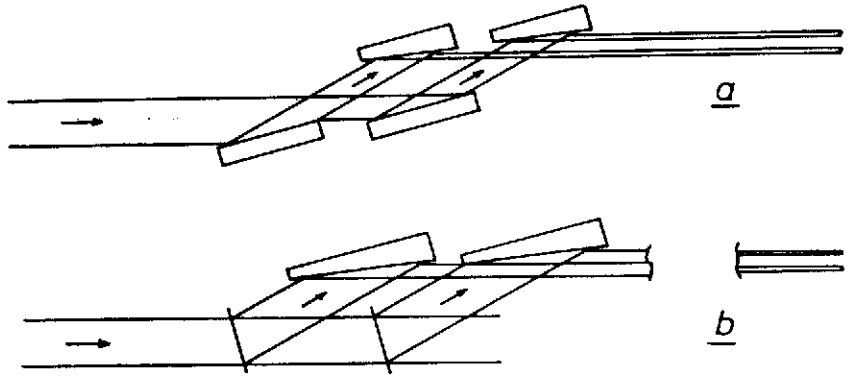

Figure 1.4: Double crystal monochromator: (a) Beam splitting by Bragg crystals, (b) beam splitting by Laue crystals.

coupled via an image intensifier to a photodiode array by special glass fibre optics.

At Tsukuba different ways of 2D imaging with image converters and so-called storage plates are investigated.

At Siegen a multiwire chamber with a very high count rate for single photon counting capable of recording two lines simultaneously is under development.

About all these different detectors and others which have been proposed for SYRDA more details are presented in individual contributions throughout the 1st Frascati Meeting on Synchrotron Radiation Applications to Digital Subtraction Angiography /9/.

Chapter 2

The NIKOS Experimental Apparatus

2.1 Introduction

NIKOS consists of five main elements: a two beam double crystal monochromator, a scanning device, a two line photodiode detector, a computer system for data acquisition and image processing, and a storage ring as a X-ray source (Fig. 2.1). Until now all investigations have been performed at the topography station at HASYLAB. This station is at a distance of 34 m from the source and receives synchrotron radiation from a bending magnet of the electron storage ring DORIS. The maximum horizontal beam aperture is 50 mm.

In the following first the present set-up is described and then some details of the future development are given. After some tests of an image converter/TV system and an energy switching monochromator (see chapter 3) we decided to implement a line scan system with two stationary beams which are recorded simultaneously. In our mind this two beam set-up seems to be the most suitable for dichromography since it is perfectly adapted to the beam geometry at a synchrotron source, has good scatter rejection and no oscillating parts.

2.2 The Double Beam Monochromator

The incident white synchrotron radiation beam is split into two monochromatic output beams by two Ge(111)-crystals. The first crystal reflects a beam with the energy E_1 from the lower part of the incident beam, the second reflects a beam with the energy E_2 from the upper part. The germanium plates are 60 mm wide and 80 mm long each. The Bragg angles for reflection are 3.29° (E_1) and 3.26° (E_2), respectively. The bandwidth of the two monochromatic X-ray beams is about 75 eV each, the energy separation of the beams is 300 eV. Each crystal is followed by a second asymmetrically cut Ge(111)-crystal that reflects the monochromatic beams back to the horizontal direction. The parallel setting of the two crystals within a few seconds of arc is controlled by a piezoceramic. We chose two independent crystals per beam to be able to minimize the fraction of higher harmonics (99 keV, 132 keV) in the monochromatic beams which

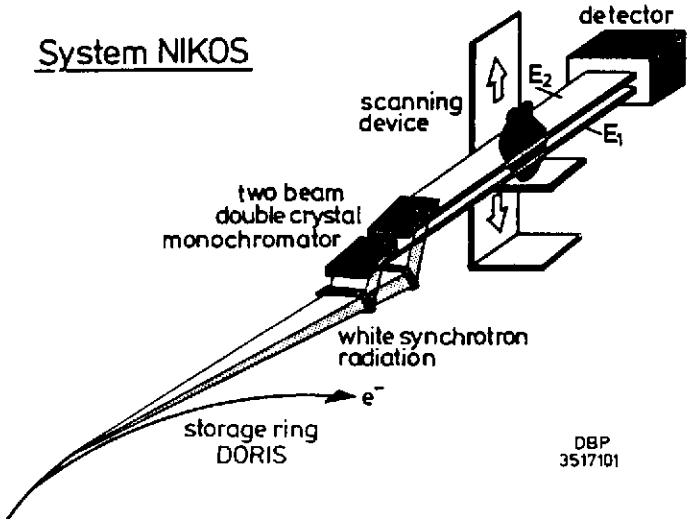

Figure 2.1: Experimental scheme.

would otherwise reduce the iodine contrast in the subtracted image. The center distance between the two 0.5 mm high X-ray beams in front of the investigated dogs was 2 mm, the beam width 45 mm. The flux at that point was $1.4 \cdot 10^9 photons/(mm^2 s)$. During the scan this flux may change by about 10% due to beam fluctuations in the storage ring. Therefore it is monitored by two phosphors scraping the beams from one side. Their light output is coupled into the detector by glass fibre cables.

It is planned to exchange the two first crystals by thin Laue case crystals (reflecting netplanes perpendicular to the surface). This has the advantage, that the monochromator is vertically focusing and less sensitive to vertical beam oscillations.

We shall use a combination of Si (111) Laue crystals and Ge (111) Bragg crystals which gives an excellent rejection of higher harmonics. The difference in Bragg angle results in an angular deviation of 0.28° of the monochromatic beams from the incident beam. The focal length of the double crystal arrangement is controlled by the asymmetry of the second Bragg crystal.

The thickness of the Laue crystal very much affects the reflectivity due to the interference of two wavefields inside the crystal, the so-called Pendellösung effect. The optimum thickness for a photon energy of $33keV$ is $31\mu m$. With such a thickness absorption can be neglected and about 70% of the Bragg case reflectivity is reached. As the beam is used twice a net gain of 40% can be achieved. The mechanical stability of such a thin crystal is ensured by leaving a thicker frame around the thin reflecting part (Fig. 2.2)

Very recent experiments with the new wiggler W2 indicate that a laminar stream of helium gas should be sufficient to cool the thin parts of the crystals being exposed to the white wiggler beam. Several of these crystals have been fabricated and tested. By selection specimen can be found with good quality for our purpose.

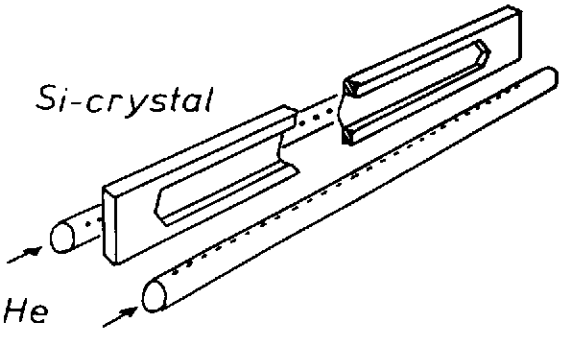

Figure 2.2: A sketch of the Laue crystal

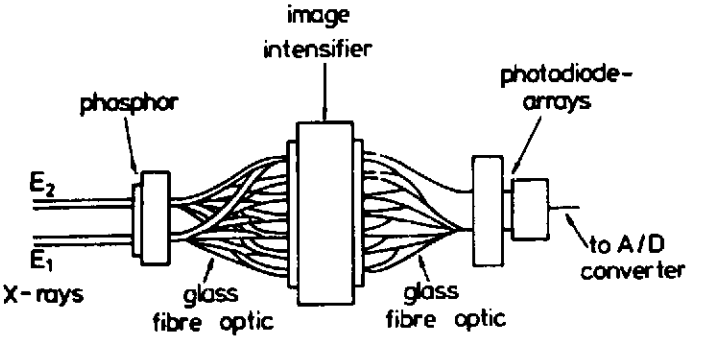

Figure 2.3: The two line photodiode detector.

2.3 The Detector

The general design of the detector is shown in Fig. 2.3. It consists of a phosphor screen, an image-intensifier and a photodiode array, all these components being coupled by means of special fibre optics. The two X-ray beams generated by the monochromator are converted to visible light by means of a phosphor layer. This layer consists of two rows of $Gd_2O_2S:Tb$ powder, one for each X-ray beam with a center distance of 2 mm. The dimension of each row is $63 \times 0.5mm^2$ thus constituting of 126 pixels, $0.5 \times 0.5mm^2$ each.

The optical light output of each phosphor pixel is transferred to an image intensifier by means of a glass fibre bundle. The above mentioned two monitor phosphors are coupled to the image intensifier by two additional fibre bundles thus also monitoring the gain of the image intensifier.

The image intensifier is required to enhance the light level of the phosphor screen to the needed intensity level at the photodiode. We chose a double stage proximity

focused image intensifier (Proxitronic Proxifier BV 2543 MX 35) having zero distortion and a gain factor of 120. To get minimum crosstalk the 256 incoming fibre bundles are distributed over the whole active input area (25 mm diameter).

A second set of 256 glass fibre bundles is positioned at the output face of the image intensifier to collect the intensified input signals. In this way every bundle of the second set just carries the information from one phosphor pixel. Their output end is formed to give a cross-section of $0.1 \times 2.5mm^2$ to match the photodiode size.

The photodiode array is a Reticon RL 1024 SF chip consisting of 1024 photodiodes each having a $0.025 \times 2.5mm^2$ input area. The second fibre bundles precisely packed side by side to form a single line are coupled to the Reticon chip. In this way every pixel of the phosphor screen covers four photodiodes. By shifting the first of these diodes onto the borderline between neighbouring glass fibre layers and only integrating over three diodes the crosstalk was further minimized.

A modified Reticon standard evaluation circuit is used for electronic readout. The internal readout trigger was replaced by an external one, which is generated by a linear transducer of the scanning device every 0.5 mm of translation. The clock frequency was increased to enable readout times of 2 ms per line. The output signals were amplified to an appropriate level for the following 12 bit, 0.5 MHz ADC (Datel ADC-817). This first detector version reached an overall detective quantum efficiency of 0.2 and a dynamic range of 1:1000 /10/. With a longer readout time (10 ms per line) a dynamic range of 1:8000 was achieved.

A new detector with two phosphor screen lines $125 \times 0.5mm^2$ each is under construction. With the increased number of pixels a slight geometric modification to the first glass fibre optic will allow for the addition of a second image intensifier and a second photodiode array. The gain factor of the intensifiers will be raised to about 500. The readout electronic is completely redesigned to enable readout times of 1 ms per line and to enlarge the dynamic range. This new version should then reach 0.6 detective quantum efficiency.

Chapter 3

Recent Results at HASYLAB

3.1 Introduction

End of 1981 at HASYLAB in Hamburg the investigations for non-invasive coronary angiography with synchrotron radiation were started. Today our group is in the fourth phase of this work. The four phases are:

1. From December 1981 to 1983 tests with phantoms and excised pig hearts were performed in a $2cm$ wide beam using a fast switching monochromator and a conventional image converter area detector (**Sirecon BV**) /5/.

2. In 1984 and 1985 construction and tests of the system **NIKOS 0** in a $2cm$ wide beam were carried out. The system included the prototypes of the two-beam double-crystal monochromator and a new detector using an image intensifier and a photodiode array. The tests were finished with the first in vivo investigation of a dog in September 1985.

3. In 1986 the system **NIKOS I** was constructed and tested in a $4.5cm$ wide beam. The detector consisted of an image intensifier, a photodiode array, and a special glass fibre optic. During this phase in vivo investigations of 7 dogs took place /11/.

4. Since the beginning of 1987 the system **NIKOS II** is under construction. It will be suited for investigations of humans using a $12cm$ wide beam.

In the following we will shortly present the experience we gathered during the first 3 phases of our work and the conclusions for the forthcoming work. All our experiments have been performed at the topography station at HASYLAB. This station receives synchrotron radiation from a bending magnet of the storage ring DORIS. During most of the experiments DORIS was running between 5.0 and $5.3GeV$ electron energy and 20 to $40mA$ current. This results in an incident photon flux at $33keV$ of about $4 \cdot 10^8 phot/(mm^2 \cdot eV \cdot s)$ (calculated for a point source). The maximum horizontal beam aperture is $50mm$.

3.2 Some Results of the First Phase

In this phase we used a commercially available detector which consists of a TV camera optically coupled by lenses to an X-ray image converter. Its characteristics are a $100mg/cm^2$ CsI phosphor screen, $16cm$ input screen diameter, a P20 output phosphor, and a standard $50Hz$ interlaced BAS video output. Horizontal and vertical pixel pitch were $0.5mm$ and $0.33mm$, respectively.

The TV camera has been equipped with either a Saticon or a Hivicon tube that mainly differ in temporal response. The Saticon shows an **afterglow** of 15% after $60ms$, the Hivicon of 50% after $100ms$.

The **spatial resolution** was measured by imaging a tungsten wire of $1.5mm$ diameter. In the central pixel we still got around 10% intensity and the profile was smeared out to five pixels ($2.5mm$) on a 75% signal level and to seven pixels ($3.5mm$) on a 90% level.

The **response function** of the image converter was determined. For this purpose the BAS-signal of the TV camera was digitized with 8 bit resolution. A flux of $10^4 phot/pixel$ led to saturation above 200 greylevels. Aiming at a noise level of 1% we shall have to detect at least $2 \cdot 10^4 phot/pixel$. Behind lung tissue this results in more than $10^5 phot/pixel$. This number is far beyond the specification of the system assuming $1ms$ integration time per pixel. Siemens specifies a linear response of the image converter up to $100mR/s$ corresponding to approximately $5 \cdot 10^3 phot/(pixel \cdot ms)$.

During continuous exposure the lowest measured **noise** was 2% of the signal. Due to afterglow the noise is reduced as compared to a single frame exposure. Hence for our application noise would be more than 2% whilst only 1% is tolerable.

Due to the **presence of iodine** in the input phosphor we measured a decrease of 34% in yield for X-ray photons with energies just below the K-edge with respect to those just above the edge. Below the K-edge the input phosphor only absorbs 50% of the incoming radiation.

Using $D = \frac{maximum\ output\ signal}{noise\ at\ signal\ levels\ with\ SNR=3}$ for the definition of the **dynamic range** we measured $D = 85$. In our application it would be reduced to less than 30 by the K-edge yield variation as well as the noise enhancement for single frame exposure.

Using an area detector instead of a line scan system increases the amount of detected **scattered radiation** thus giving a worse signal-to-noise ratio (SNR). Measurements with several different synchrotron beam cross sections showed scattered fractions (detected scattered radiation / total detected radiation) behind a water-filled lucite tube ($175mm$ edge length) between 0.35% and 1.7% for beam cross sections between $3x3mm^2$ and $24x3mm^2$. Extrapolation to the full cross section of a synchrotron beam of $100x7mm^2$ yields an expected scatter fraction of 8%. A larger beam width would increase the scatter fraction even further. This is indicated by experiments on X-ray tubes which showed a scatter fraction up to 90% in the neighborhood of the lungs /7/.

Because of these measured data we decided that this system was not suitable for our application without major changes though the idea of using a commercially available detector with widespread use was fascinating. The main reasons for our decision were low dynamic range, long afterglow, high scatter fraction, low X-ray absorption below the K-edge, and count rate limitation of the system. So we started the development

and construction of the detector which is used in the system NIKOS. Its parameters are optimized for our application.

In the first phase we used a fast switching double crystal monochromator /12/. For the crystals two $60mm$ wide and $80mm$ long plates of germanium were installed (Ge 220 reflection). A piezoceramic controls their parallel setting. The crystals are mounted in a rectangular frame, the angular position of which with respect to the incident beam defines the transmitted energy and is adjusted by a loudspeaker coil. A DC bias sets the monochromator to the K-edge position, whereas the AC component of the coil input wobbles the monochromator around its center position at frequencies of several hundred Hertz. Its amplitude can be chosen in such a way that the transition time from one energy to the other is only 10-15% of the full cycle.

The tests showed that the monochromator can be operated up to frequencies of $100 - 150Hz$ without significant loss of performance. But frequencies up to $1kHz$, as required for the acquisition of images within a heart cycle, are not obtainable with this device without major improvements. Therefore a new two-beam double-crystal monochromator without moving parts was constructed for the system NIKOS.

3.3 In vivo Investigations with the Systems NIKOS 0 and NIKOS I

The main parts of the system NIKOS - monochromator and detector - are described in detail in chapter 2 and in ref. /13/. For tests of the system we again imaged different phantoms (tubes in lucite blocks) and excised pig hearts. After having determined most of the parameters with these not moving structures we started in vivo investigations of dogs.

The aim was to find out the limitations coming forth by the method or the set-up, respectively. So the goal was not to produce images as brilliant as possible but to check how the images of the coronary arteries look like under the poorest conditions we expect in the final version of the system.

Until September 1986 eight dogs were investigated. The weight of the dogs was $10 - 23kg$, the soft tissue to be penetrated $12 - 15cm$. These relatively small dogs have coronary arteries of only $1.5mm$ diameter in the root part and of $1mm$ or less in parts not superposed by the aorta (see Fig.3.1). So we got extreme conditions for the tests of the system NIKOS.

Fig.3.3 shows the images with energy E_1 and E_2, respectively, and the subtraction image of one single scan in the $4.5cm$ wide beam. In Fig.3.2 the expected anatomical situation for this scan is presented. The following data of the scan are similar to those of all other scans we performed.

The dog was positioned on the back and anaesthetized. $7ml$ of contrast medium (Urografin$^{(R)}$ 76%) were applicated within 1 second via a heated tube and a catheter positioned in the vena cava inferior. This results in about $16mg/ml$ of iodine in the aorta or $1mg/cm^2$ in the right coronary artery (RCA) visible in the image, respectively. The scan was started ECG-triggered $21s$ after injection of the contrast medium. The scan velocity was $18.2cm/s$. This results in an exposure time per line of $2.7ms$. The

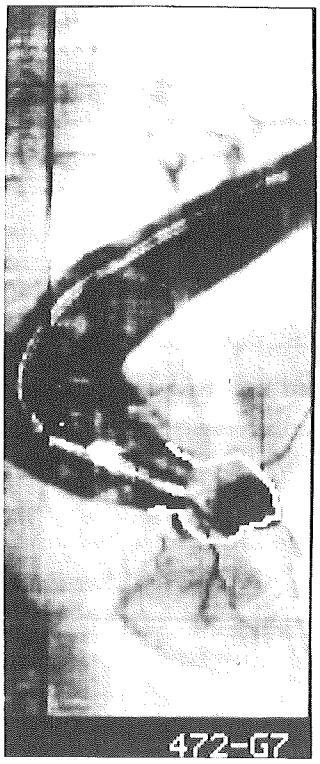

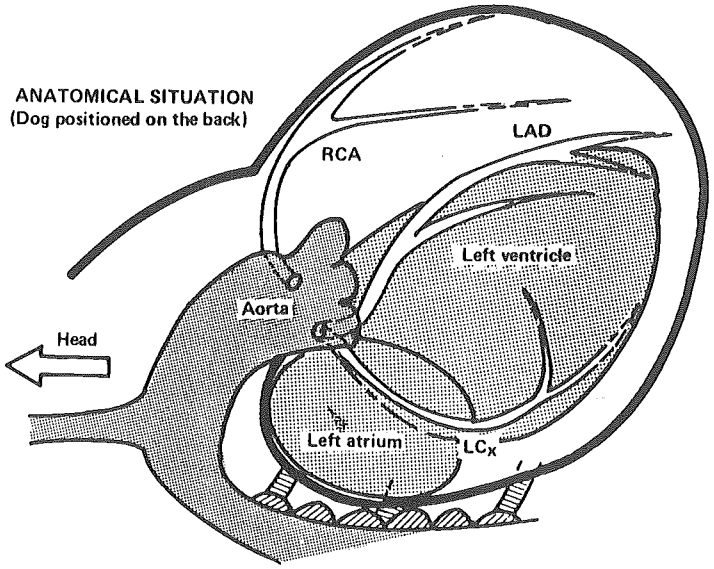

Fig. 3.1: Aorta of a dog (width of the scan: $45mm$). The contrast medium is applicated into the aorta. The white line gives the contour of the aorta in the part not opacified. The right coronary artery is visible below the aorta.
Fig. 3.2: Expected anatomical situation in the scan shown in Fig.3.3.

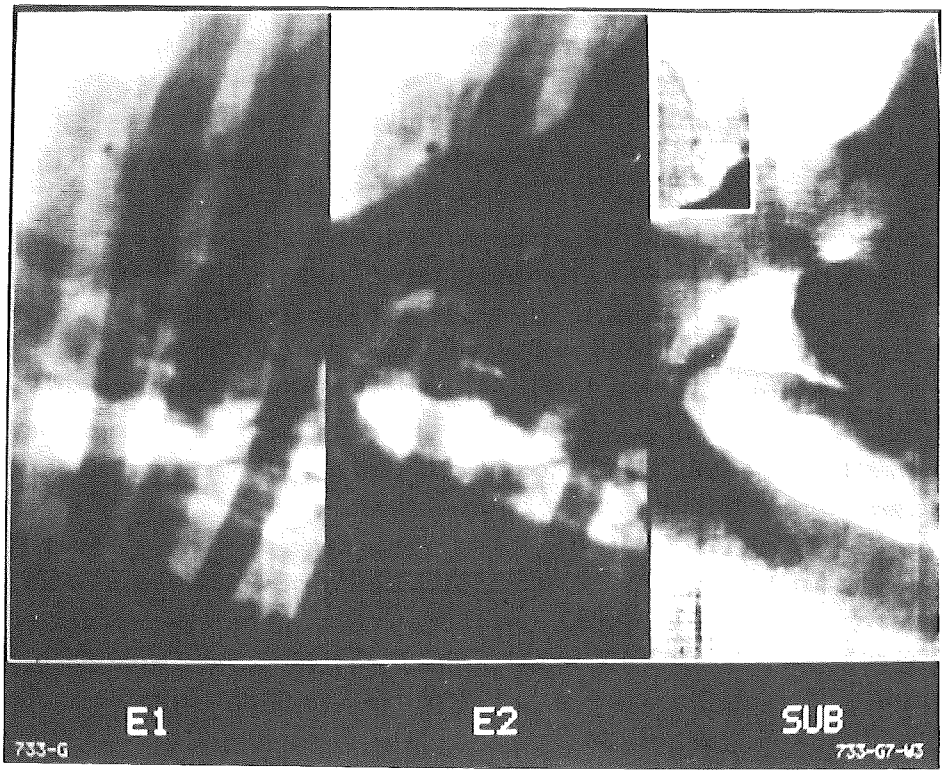

Fig. 3.3: Images with energy E_1 and E_2 and the corresponding subtraction image.

scan (176 lines) was therefore finished within $480ms$. We measured a skin dose of $0.2rem$ per scan by placing small thermoluminescent crystal dosimeters at the skin of the dog.

In this case we used the two beam single crystal version of the monochromator and the detector of NIKOS I. Details of the computer system and the image processing are given in chapter 5 and in ref. /14/.

The RCA ($1mm$ diameter) is visible and gives a signal of 3%. But the image clearly shows that $SNR = 2$, which is true for this artery, is too small and has to be increased for imaging arteries of $1mm$ diameter. In this projection the left coronary arteries (LAD and Cx) are superposed by the left atrium und left ventricle. It was not possible to figure them with the help of edge detection algorithms.

Images of the same quality we got from further scans and investigations. So with NIKOS I it was shown that the system is able to figure moving structures down to $1mm$ diameter and with opacification by $1mg/cm^2$ of iodine after rapid intravenous injection of contrast medium, using dogs ($12cm$ of soft tissue) for the investigations. But the SNR in the images and the flux of the incoming beam have to be increased before patients ($20cm$ of soft tissue) can be investigated.

3.4 Implications for the System NIKOS II

It is planned to use the system NIKOS II for the investigation of patients. For this purpose the SNR must be increased by a factor of 2. A scan velocity of $50cm/s$ will be necessary (factor 3). Because about $20cm$ of soft tissue have to be penetrated instead of $12cm$ another factor of 16 must be gained. In total this results in a necessary gain factor of 100.

This factor we shall get in part by the installation of a new **wiggler beamline**. The wiggler magnet has already been installed in the storage ring DORIS. It has 20 poles and a field of $1T$. The tests are under way. By this wiggler and the changes in the monochromator the flux in front of the patient (today $1.4 \cdot 10^9 phot/(mm^2 \cdot s)$) will be increased by a factor of 35 to $5 \cdot 10^{10} phot/(mm^2 \cdot s)$.

Another factor of 3 we will gain by changes in the **detector** for NIKOS II. The input phosphor and the image intensifier will be replaced. By this the DQE of the detector is increased from 0.2 to 0.6. The detector now under construction will have a width of $12.5cm$ and new readout electronics. The electronics will allow a readout time per line of $1ms$ (today $2ms$) and hence a scan velocity of $50cm/s$. The electronical noise should be decreased by a factor of 3 with the new system.

Up to now we used for data acquisition and image processing two **computers** (PDP11/34 and PDP11/40) linked via PADAC (in-house system of DESY). The two machines are connected to the DESY computer center. They are exchanged against a new PDP11/73 and a MikroVAX workstation II/GPX. On the workstation we shall install the image processing system of the Dept. of Computer Science in Medicine of the University-Hospital Eppendorf (IMDM).

All these changes and improvements of the system will lead to the system NIKOS II. With this system we shall repeat the in vivo investigations of dogs and start investigations of patients in 1988.

Chapter 4

Projection Angles for Intravenous Coronary Angiography

4.1 Introduction

Visualization of the coronary arteries can be achieved by rapid **intravenous** contrast bolus injection if synchrotron radiation and digital subtraction angiography in energy-subtraction mode is used to allow detection of iodine containing structures only /15/. The minimal mass density of iodine must be $1mg/cm^2$ to allow detection of coronary arteries of $1mm$ diameter. This results in an iodine concentration of $10mg/ml$, which can be achieved by a peripheral intravenous bolus injection of $10 - 20ml$ Urografin$^{(R)}$ 76% ($370mg\ iodine/ml$) /8/. Our animal experiments clearly have shown that after rapid intravenous bolus injection of $0.3ml/kg$ body weight of Urografin$^{(R)}$ 76% right heart and lungs are free of iodine at the time, when left atrium, left ventricle, aorta and coronary arteries are opacified by iodine /11/. But even then important parts of the coronary arteries may be superposed by iodine structures of the left heart chambers or aorta. Therefore, it was necessary to find out projection angles for the investigation of patients, where the artery of interest is moved into a clear field.

4.2 Material and Methods

We have studied 22 human hearts excised in toto between the first and latest third day after death and filled left ventricle, ascending aorta and the coronary arteries with contrast material ($BaSO_4$ in gelatine, Fig. 4.1.). The weight of the hearts ranged between 300 $661g$ (mean $442 \pm 84g$). 9 hearts revealed the left ventricle in systolic contraction, 6 hearts in diastole, 7 hearts showed an intermediate contraction pattern of the left ventricle. The hearts were mounted in a cardanic suspension and examined under conventional X-ray control (Fig. 4.2). Depending on the individual heart size the left side of the hearts was filled with a volume of $90 - 200ml$ (mean $142 \pm 38ml$).

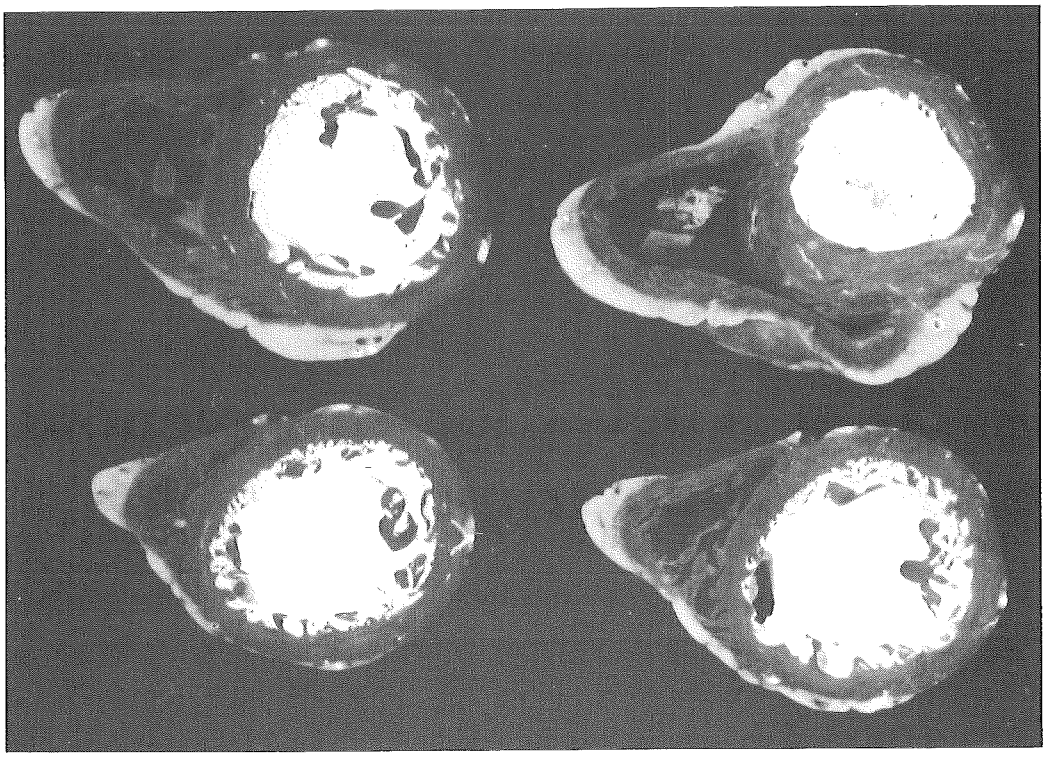

Figure 4.1: Slices of a human heart, left ventricle and coronary arteries filled with $BaSO_4$, right heart free of contrast material.

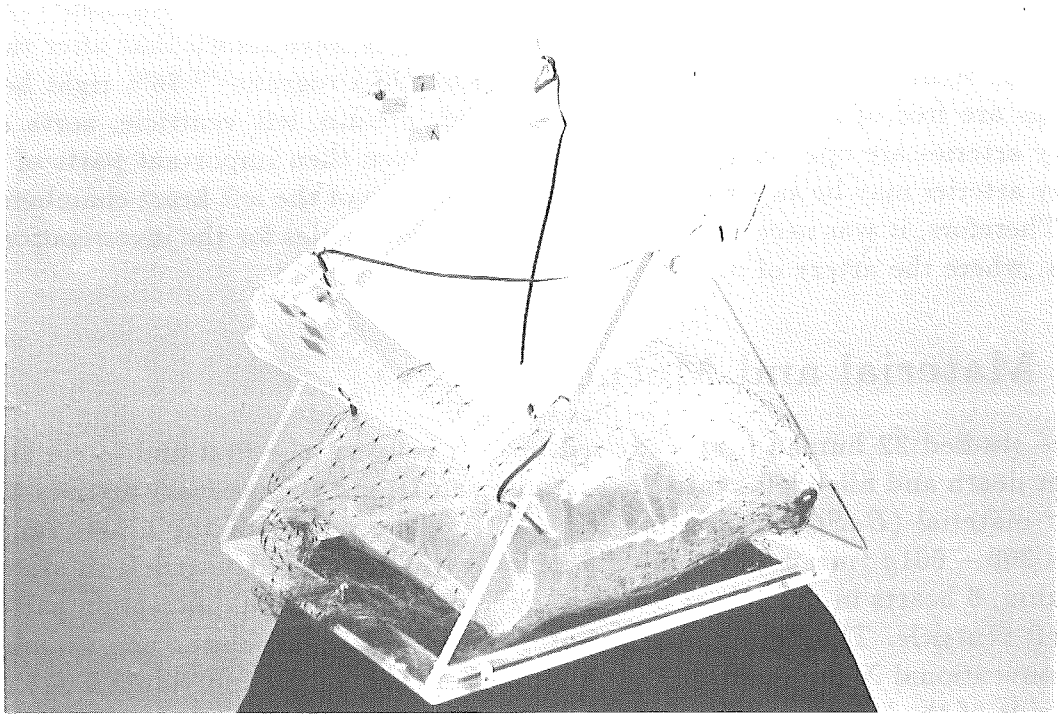

Figure 4.2: Cardanic suspension, which allowed graded rotation of the hearts in all directions in steps of 10^o. Air-bag below to simulate thoracic gas volume.

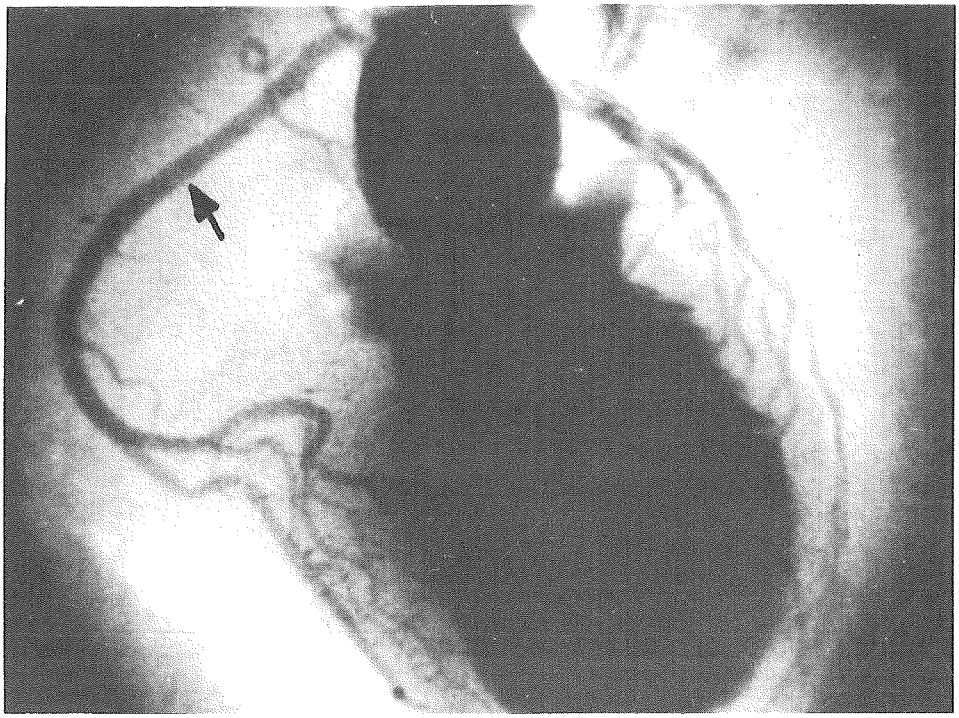

Figure 4.3: Left ventricle in diastole, left atrium contracted, complete visualization of the right coronary artery at the left side of the figure (arrow).

4.3 Results

20 of the 22 hearts were of sufficient quality to allow detailed study. Fluoroscopy showed 3 hearts with a left dominant coronary type, 8 hearts with a right dominant coronary type and 9 intermediate.

128 different projections were analyzed up to 50° right or left anterior oblique rotation or ±50° cranio-caudal rotation. Higher degrees of rotation would lengthen the transmission distance through soft tissue and attenuate the synchrotron radiation too much.

In 20 out of 20 hearts it was possible to visualize the right coronary artery without superposition. In 90% of the hearts the left anterior oblique (LAO) 40° rotation and cranio-caudal (CC) 20° angulation showed the complete right coronary artery without superposition (Fig. 4.3).

Combined with the LAO−40° and CC−30° or 0°-angulation the right coronary artery could be seen in all cases. Preferable was having the left ventricle in diastole and the left atrium contracted, so the origin of the right coronary artery out of the bulbus aortae could also be seen.

The left anterior descending coronary artery was best seen in the right anterior oblique (RAO) 40° rotation and CC−20° angulation (17/20 hearts, 85%) (Fig. 4.4). The second best projection was RAO 40°, CC 10° (16/20 hearts, 80%).

As it could be expected, it was difficult to get the left main stem and the proximal part of the left circumflex coronary artery free of superposition with other iodine containing structures. Best angulation for the left circumflex coronary artery were LAO 40°, CC 30°-rotation or LAO 40°, CC 20°-rotation (Fig. 4.5).

Main stem was seen only in 3 out of 20 hearts, possibly due to incomplete filling of the left atrium.

Figure 4.4: Left anterior descending coronary artery at the right side of the figure (arrow).

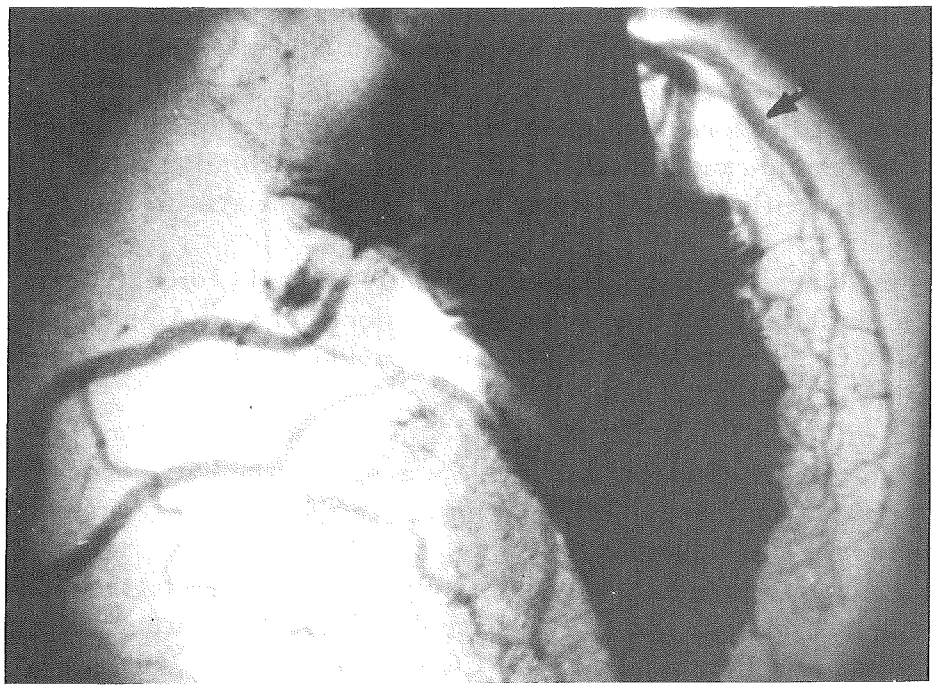

Figure 4.5: Visualization of the complete right coronary artery, parts of the left anterior descending coronary artery superposed by the left ventricle and the marginal branches of the circumflex coronary artery (arrow).

4.4 Conclusion

Detailed analysis with stepwise rotation in 10° of human hearts with the left ventricle, left atrium, bulbus aortae and coronary artery system filled with contrast material revealed that it is possible, with 2 to 3 different projections to examine the interesting parts of the coronary arteries free from superposition of structures of the left heart and aorta. The full range of image enhancement techniques will be necessary, to figure out the left main stem (normally with a diameter of $5mm$) overlapped by either aorta (diameter $40-50mm$) or left atrium (diameter $40mm$). This was also found true for the proximal part of the left circumflex coronary artery, which lies in the atrio-ventricular groove.

Chapter 5

Image Processing of SYRDA Pictures

5.1 Introduction

The groups working in the field of coronary angiography with synchrotron radiation installed systems with different components, especially detectors. This implies that details are different in the following image processing, too. Therefore we only present the more common considerations which should be of interest to all groups. If numbers are necessary for examples we use the data and parameters of the system NIKOS. Not all of these numbers are relevant for each of the other systems.

At the beginning of this presentation it should be stressed, that in medicine one always has to find a compromise between the quality of images and the radiation dose one allows for the patient. If the physician decided, he had to see vessels with a diameter of $1mm$ or more, it is not necessary to figure smaller vessels with good quality. Then the system has to be optimized for this purpose, that means for figuring vessels of $1mm$ diameter with good quality and with as little radiation dose for the patient as possible.

The following considerations for the image processing of SYRDA images are based on the calculations presented in chapter 1. Arteries of $1mm$ diameter give a 3%-signal. Therefore the quantum noise should be at most 1% in order to get a signal-to-noise ratio (SNR) of at least 3. The electronical noise and other uncertainties in the system must be less than 0.1%. This is a hard demand to the systems. For example in the system NIKOS the necessary corrections to the unprocessed E_1- and E_2-images amount to 60%, most of it being fixed pattern noise corrections.

5.2 Image Processing of the Raw Data

To give an impression of the necessity of image processing, Fig.5.1 shows two subtraction images, the first one without image processing. To get images of good quality the following corrections to the raw images should be performed:

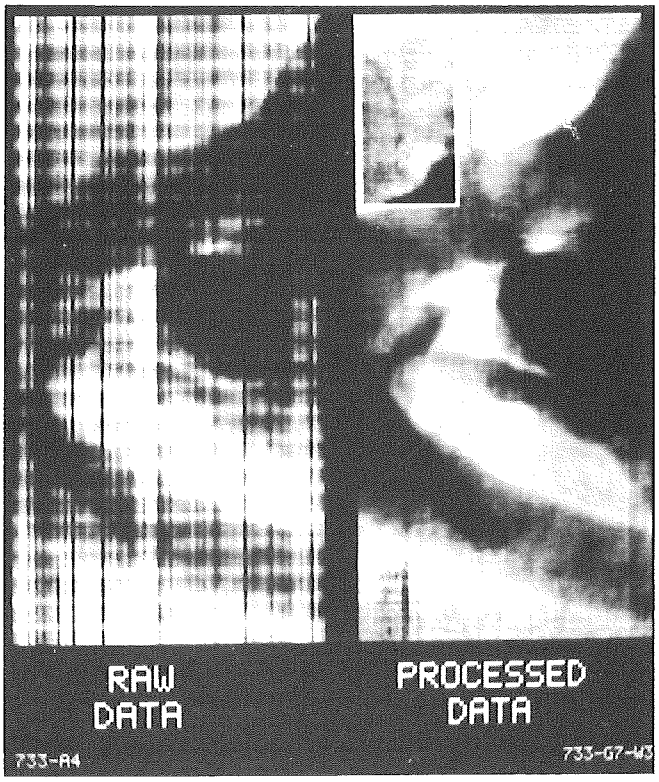

Fig. 5.1: Two subtraction images from the same scan. The first image was subtracted without use of image processing algorithms. The vertical artifacts arise from fixed pattern noise, the horizontal ones mainly from beam fluctuations.

- The images have to be corrected for **fast fluctuations in the incident beams.** For example at DORIS they can reach 10%. These fluctuations have to be measured. Usually they are different in the two beams with energy E_1 and E_2, leading to their enhancement after subtraction of the images.

- When using a line scan system the **irregularities of the scanning device** have to be measured carefully and corrected for.

- Depending on the synchrotron radiation source and the monochromator the beams have different higher harmonic portions (photons with energies of $66k\epsilon V$, $99k\epsilon V$ etc.). For a given set-up they may even differ for the two beams. This leads to corrections for **beam hardening effects**. (Not yet done for the presented NIKOS images.)

- The **dark current** of the detector must be determined and subtracted.

- If the detector uses different channels for registration of the E_1- and the E_2-image (e.g. a two-line detector) corrections for **fixed pattern noise** must be performed. During the in vivo investigations of dogs with NIKOS the necessary data for correction were sampled in every scan by using 25 lines of the scan for imaging a reference aluminium plate of $15mm$ thickness.

  This procedure will not be possible during investigations of patients. Therefore we tested a simple algorithm in order to remove the artifacts due to fixed pattern

noise in the subtracted image without measured information. In the algorithm step by step each column x_i is adjusted relative to column x_{i-1}, starting at column 2, in the following way: The difference in greylevel of each corresponding pixel in the two columns is determined. An automatic peak finding algorithm isolates the most prominent peak of the resulting distribution. The shift of the peak relative to zero gives the value for the adjustment of x_i.

The same procedure is used for line normalization. The resulting images have comparable quality to those processed with measured correction values.

- The following two corrections should be of interest only for some of the existing detectors.
  - The **afterglow** from line to line was measured in NIKOS to be 6.7% for the next line. Appropriate corrections to the data are made but did not increase the quality of the images.
  - Also the horizontal **crosstalk** from pixel to pixel due to the phosphor screen, glassfibre optics, Reticon chip and electronics in the detector of NIKOS was measured for each pixel of the detector. The measurement showed a crosstalk of about 5%. The values for each pixel are corrected by deconvolution of the corresponding matrix. This is a rather stringent method resulting in artifacts in the image. Therefore a better algorithm must be found.
- The **presentation** of the images is of great importance because very small structures must be visible in the neighbourhood of large structures like aorta and left chambers. In images with low SNR pseudocolours for the presentation have no positive effect, on the contrary they confuse the observer. The images should be figured on a black/white monitor using greylevel adjustment. Experience shows that best presentation with a fixed algorithm is got by cutting off 3% of the highest and 3% of the lowest grey values and afterwards setting the minimum value to 0 and the maximum value to the maximal possible value of the monitor (normally 256). The result is a good overview image. Now a region of interest (ROI) for the small structures can be selected interactively. In this ROI the greylevel adjustment procedure is repeated.

5.3 Image Simulation

The computer system used for NIKOS is based on two computers connected via PADAC (in-house system of DESY). From a PDP 11/34 experiment control, data acquisition, data storage, and image processing is coordinated (see Fig.5.2). A PDP 11/40 is used for the control of the complete experimental set-up. The two computers are linked to the IBM 3084Q of the DESY computing center for preprocessing of the data. A more detailed description can be found in ref. /11/.

The complete system is also connected to the central computer (VAX 11/780) of the Dept. of Computer Science in Medicine (IMDM), University Hospital, Hamburg

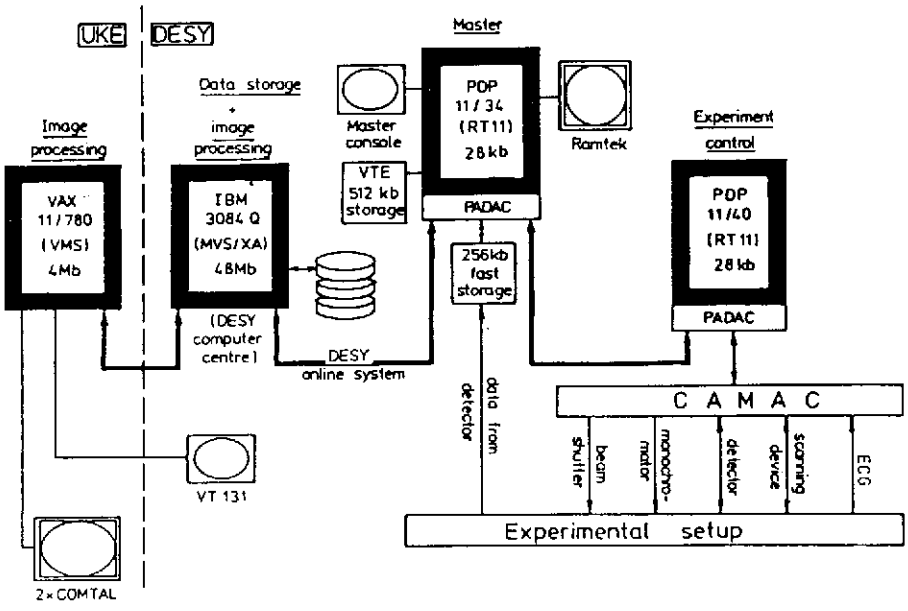

Fig. 5.2: The NIKOS computer system

(UKE). After preprocessing at DESY the images are transferred to the image processing system of the IMDM for more sophisticated evaluation. Besides the subroutine package developed at the IMDM this image processing system includes SPIDER /16/.

Using such a computer network not only evaluation of the measured data and processing of images from the investigations is possible but also simulation of images in order to get parameters and constraints for the experimental set-up. In the following we present three examples:

- It was decided that arteries of $1mm$ diameter or larger have to be figured. Therefore it must be tested which pixel size is necessary for this application. Fig.5.3 shows that arteries of $1mm$ diameter are clearly visible with a pixel size of $0.5 \times 0.5mm^2$, if they are not superposed by larger structures. In the image with smaller pixel size the quality of the edges of this artery is not remarkably higher. So today we do not propose to decrease the pixel size of $0.5 \times 0.5mm^2$ which would result in an quadratic increase of the radiation dose for the patient. Further simulations and investigations of patients have to show to what degree stenoses will be visible in these $1mm$ arteries. The physicians must see stenoses in these small vessels down to 70% cross sectional occlusion.

  The pixel size of $0.5 \times 0.5mm^2$ leads to a 256×256-matrix for the image of the complete heart. This spatial resolution is not (and has not to be!) as good as that of images one gets from conventional angiography using modern image intensifiers (4 line pairs per mm), for which a digitalisation matrix between 512×512 and 1024×1024 would be adequate /17/.

  Furthermore in systems for dichromography information about the degree of stenoses is not only achievable from spatial data but also from density data. Here more research is necessary.

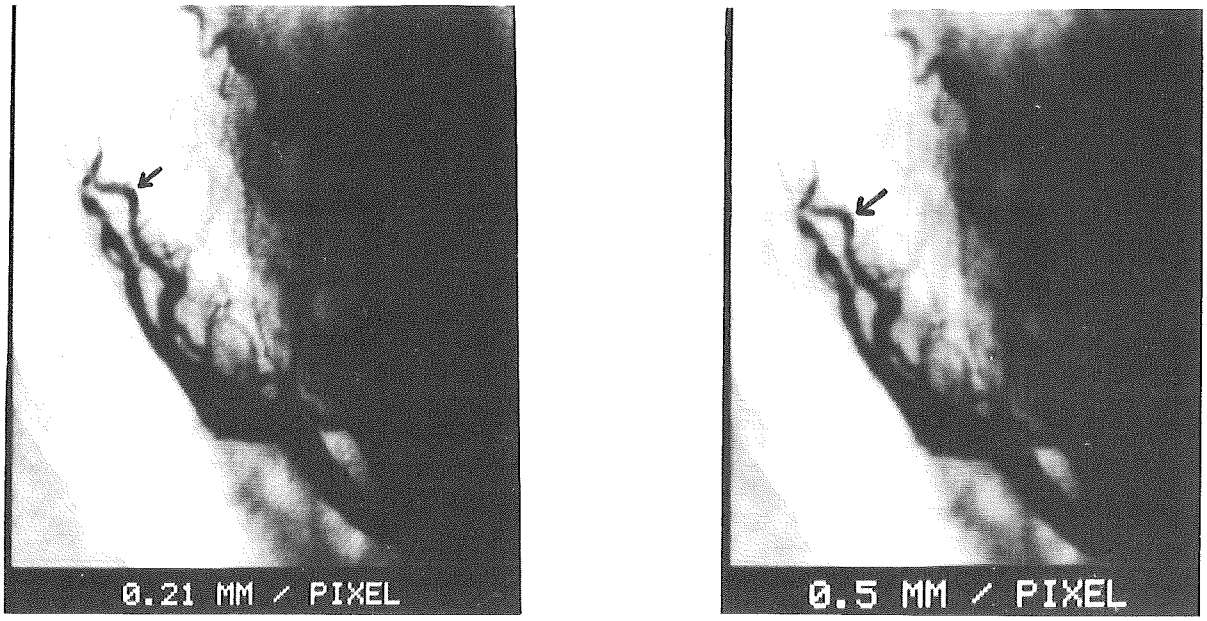

Fig. 5.3: The same image with different resolution. The arrow marks an artery of $1mm$ diameter.

- Line scan systems lead to deformation of the figured arteries because these move during the scan. It has to be determined how fast one has to scan for fear that deformation becomes relevant. Strong deformation can make believe a stenosis or can suppress an existing one.

  For these tests we digitized a cine film from an investigation with conventional equipment. The film showed a coronary artery with a stenosis. From the digitalized images we used different successive lines and composed a new image. Thus we simulated images for scan velocities between $12ms$ per line and $1ms$ per line. From these images we learned that a scan velocity of $1ms$ per line is necessary. Even that produces small deformations in the arteries if the image was taken during fast contraction of the heart. Only images, taken in the slow phase of the heart and with $1ms$ per line, are comparable to those of the original cine film.

- Of great importance is the knowledge, what SNR can be allowed in the images. In the following only images with a pixel size of $0.5 \times 0.5mm^2$ are used, and the SNR is always given for arteries of $1mm$ diameter.

  For these examinations we took a digitalized image and added noise with different selectable levels to the image by using a Monte Carlo program. Fig.5.4 shows that images with SNR=3 are rather poor and that this SNR is the smallest to be allowed.

5.4 Image Enhancement

Image enhancement algorithms must be used to figure those coronary arteries for which no projection exists where the arteries are not superposed by larger structures. So in

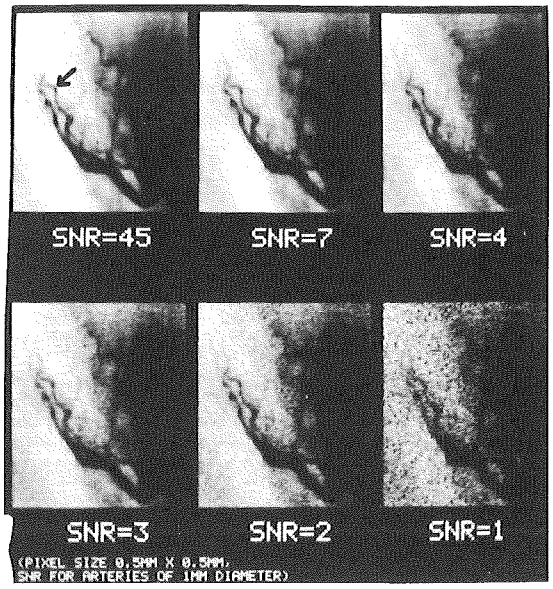

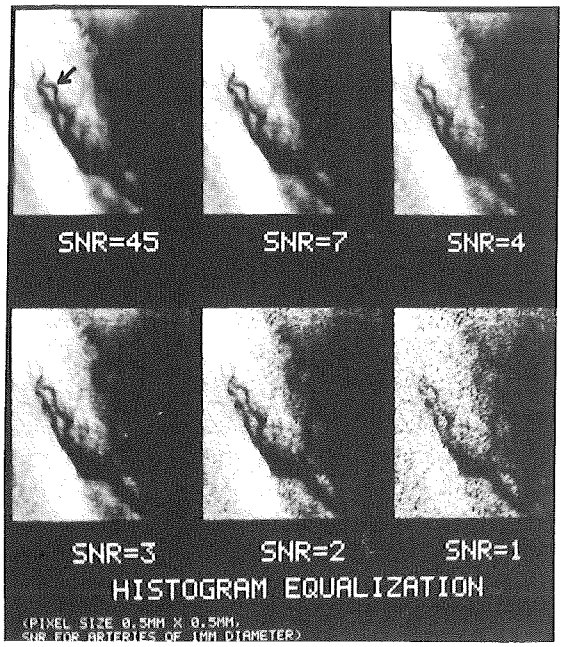

Fig. 5.4: The same image with different noise levels. The SNR is given for an artery of $1mm$ diameter marked by the arrow.

Fig. 5.5: The images of Fig.5.4 after histogram equilization (with uniform distribution).

most of the cases the main stem will be superposed by the aorta or left atrium and part of the left circumflex artery (Cx) by the left atrium (see chapter 4).

We calculated the SNR of these superposed arteries, assuming there is 1% noise in the subtracted image, what should be aimed at. Assuming furthermore an artery of $5mm$ diameter (e.g. main stem) superposed by a structure of $50mm$ filled with iodine (e.g. aorta, what is extreme because the aorta normally has a diameter of $40mm$), then this artery has a SNR of 7 (14% signal, 2% noise because of the increased absorption). If there are additional $1.8cm$ of bones (e.g. ribs), then the SNR is decreased to 3. Also SNR=3 was calculated for the Cx ($2mm$) in front of the left atrium ($50mm$, what is also extreme). Keeping in mind these numbers and using the images of Fig.5.4, we tested up to which SNR different image enhancement algorithms worked. Up to now only existing subroutines out of the image processing package of the IMDM and the SPIDER package were used. The results are preliminary, and more work has to be done in this field.

Image enhancement of the SYRDA images is possible with three different methods:

- **Histogram equilization** (see Fig.5.5): The best results we got with an algorithm for uniform distribution of greylevels proposed by Pratt /18/. Other algorithms for hyperbola distribution or Rayleigh distribution produced images of lower quality. In total these algorithms did not remarkably increase the quality of the original image.

- **Edge preserving smoothing** (see Fig.5.6): The best results we got with an algorithm for local selective averaging based on a concept of relative similarity proposed by Yokoya et al. /19/, and with an algorithm proposed by Nago et al. /20/. The images produced with these algorithms have certainly a better quality

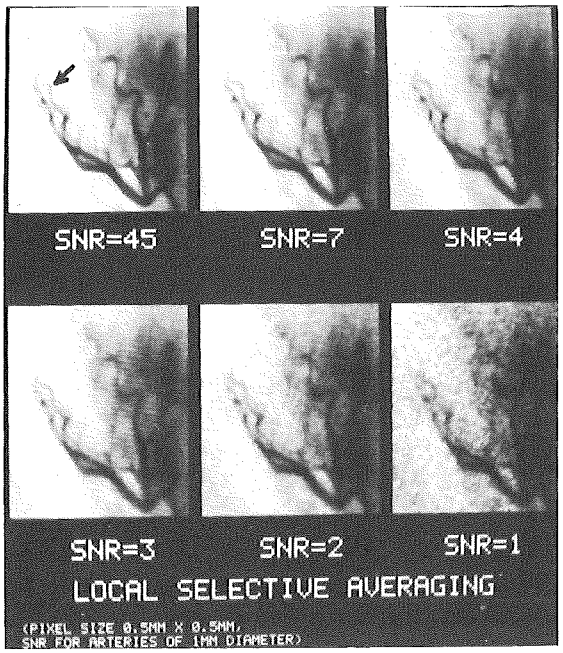

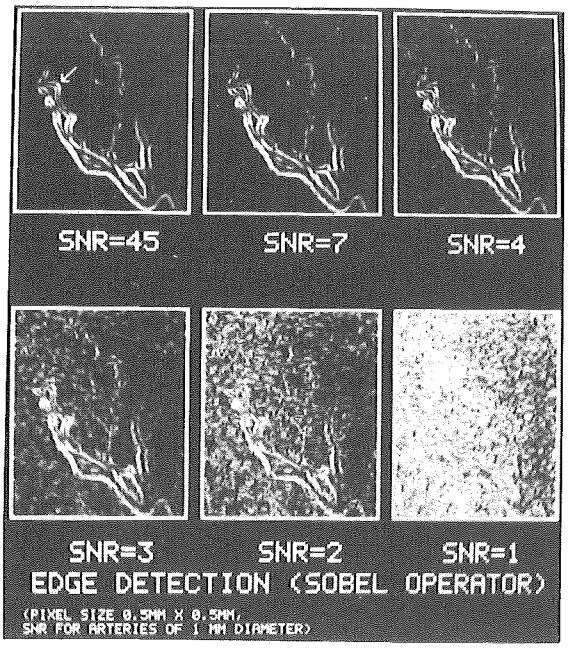

Fig. 5.6: The images of Fig.5.4 after edge preserving smoothing (algorithm of Yokoya et al.).

Fig. 5.7: The images of Fig.5.4 after edge detection (Sobel operator).

than the original images for SNR=4 and higher SNR. For SNR=3 or less gain was achieved for arteries which were hidden by large structures. With algorithms like median filtering /21/ we had no success.

- **Edge detection** (see Fig.5.7): The algorithms of Frei et al. /22/, of Hückel, and the Laplace operator produced images with bad quality. Only the Sobel operator worked well. With this algorithm the edges of arteries without superposition were detected down to SNR=4. Superposed arteries, even with higher SNR, were hardly detected.

5.5 A Computer System for Dichromography

The last but not unimportant link in the chain of devices for dichromography is the computer system. When designing this system help can come from the development of imaging systems for digital angiocardiography, designed to replace the traditional film techniques in the existing laboratories /23/. Of course, with respect to data acquisition and data storage these systems are oversized for dichromography, because they are aimed to store up to 25 images of 1024×1024 pixels within 1 second. Nevertheless the basic ideas of these systems are also true for systems installed for dichromography. In the moment there is still a large discrepancy between the obvious requirements and the digital image processing hardware and software available from the industry.

The tasks of the computer system for dichromography are data acquisition, data storage, and image processing. It is not advisable to use one (slow) general purpose computer for these different tasks. A computer network consisting of at least 3 specialized computers, one for each task, connected via a fast net (e.g. Ethernet) is in any

case better suited. In the following some remarks to the three computers are made:

- **Computer for data acquisition:** Per injection of contrast medium maximal 2 scans (2 images each) during two different heart beats are possible with line scan systems. Assuming a maximal matrix size of 512×512 per image and 16 bit per pixel (the resolution of the detector should be 12 to 14 bit) $1Mbyte$ must be read within $250ms$ resulting in a rate of $3.3 \cdot 10^7 bits/sec$. The rate can be reduced by parallel data acquisition e.g. parallel input of the 2 images. The storage capacity for the fast input storage must be $2Mbyte$ corresponding 2 scans. The transfer of the data onto the final storage medium has no temporal constraints because the time up to the next injection is not fixed.

  Furthermore this computer should optimize the parameters of the complete system (detector, projection angles for the scanning device etc.) to the geometry and the circulation of the patient. Using these parameters it controls the system during the scans, e.g.

  - readout of the ECG,
  - start of the injection,
  - control of the scanning device,
  - control of the monochromator,
  - control of the detector and data acquisition,
  - monitoring of the radiation dose,
  - control of the safety equipment.

  All data and parameters have to be added to the corresponding images into a history file.

- **Computer for data storage:** Using dichromography for routine investigations will require a large number of patients studied per year at such an expensive source in order to save costs. Assuming up to four necessary scans for one patient can be done in $15min$ and the system runs 8 hours per day and 250 days per year, then 32000 scans must be stored in 1 year. Each scan consists of 3 images (E_1, E_2 and subtracted image) with $0.5Mbyte$ each (512×512 matrix). Assuming a further factor 2 for research purpose during which images are processed and therefore duplicated, then about $100Gbyte$ of storage capacity are needed for 1 year. Compression by a factor 2 to 3 by reversible coding is possible.

  The new laser discs can store up to $2Gbyte$ per disc. Within 2 years we expect digital tape recorders with a capacity of $15Gbyte$ per tape. Larger tape cassettes will store up to $120Gbyte$.

  So the necessary hardware for a suitable Picture Archiving and Communication System (PACS) should be available when dichromography can go into routine. But up to now there are no general software solutions for such a system. The development of image database languages is only in the beginning. E.g. in the IMDM the language ISQL (=Image-SQL) using the database language SQL and the DBMS ORACLE is under development /24/.

- **Computer for image processing**: This computer must have large computing power. It should have large memory because paging in the virtual management systems is time consuming or it should have facilities for parallel processing. Response times for interactive use of the system must be in the order of a few seconds for the following tasks:

  - Simple histogramming, cuts, greylevel adjustment, setting of ROI etc. by menu driven interaction,
  - image processing including subtraction, spatial filtering, edge detection etc.,
  - access not only to image data but also to patient data, parameters of the investigation, signals like ECG etc.

  The system must include at least a black/white monitor (for presentation of the images) and a colour monitor (for research) with a resolution of at least 512×512 pixels. Hardware like trackball or mouse must be included.

  Again the necessary hardware is available but no enduser-oriented commercial software system for image processing (not to confound with a graphic system!) including image input and output and man-machine interaction facilities is on the market. Today only libraries of image processing algorithms exist, e.g. SPIDER.

Bibliography

/1/ C.P. Höppner: Untersuchungen zur Angiographie mit Röntgenfluoreszenz, Diploma thesis (in German), Univ. of Hamburg, 1985.
/2/ S.J. Riederer, D.L. Ergun, R.A. Kruger, C.G. Shaw, C.A. Mistretta: System for Automated Real-Time Generation of Higher Order Energy Subtraction Images in Digital Fluoroscopy, SPIE, Vol. 314, (1983).
/3/ E.B. Hughes, E. Rubenstein, H.D. Zeman, G.S. Brown, M. Buchbinder, D.C. Harrison, R. Hofstadter, R.S. Kernoff, J.N. Otis, A.C. Thompson: The angiography program at Stanford. NIM A246 (1986) 719.
/4/ E.N. Dementyev, E.Ya. Dovga, G.N. Kulipanov, A.S. Medvedko , N.A. Mezentsev, V.F. Pindyurin, M.A. Sheromov, A.N. Skrinsky, A.S. Sokolov, V.A. Ushakov, E.I. Zagorodnikov: First results of experiments with a medical one-coordinate X-ray detector on synchrotron radiation of VEPP-4, NIM A246 (1986) 726.
/5/ W.-R. Dix, K. Engelke, C.-C. Glüer, W. Graeff, C.P. Höppner, K.-H. Stellmaschek, T. Wroblewski, W. Bleifeld, K.H. Höhne, W. Kupper: NIKOS - A System for Non-invasive Examination of Coronary Arteries by Means of DSA with Synchrotron Radiation, NIM A246 (1986) 702.
/6/ A. Akisada, M. Ando, K. Hyodo, S. Hasegawa, K. Konishi, K. Nishimura, A. Maruhashi, F. Toyofuku, A. Suwa, K. Kohra: An Attempt at Coronary Angiography with a Large Size Monochromatic SR Beam, NIM A246 (1986) 713.
/7/ L. T . Niklason, J.A. Sorenson, J.A. Nelson: Scattered Radiation in Chest Radiography, Med. Phys. 8, 677 (1981).
/8/ W.-R. Dix, C.-C. Glüer, W. Graeff, K.H. Höhne, W. Kupper: Überlegungen zur nicht-invasiven Koronarangiographie mit Synchrotronstrahlung, DESY SR-82-24 (1982).
/9/ Proc. of the 1st Frascati Meeting on Synchrotron Radiation Applications to Digital Subtraction Angiography, Societá Italiana di Fisica (1987) (to be published).
/10/ C.-C. Glüer, Dissertation Univ. Hamburg 1986.
/11/ W.-R. Dix, K. Engelke, C.-C. Glüer, H. Jabs, W. Graeff, W. Kupper, K.-H. Stellmaschek: NIKOS - A System for Non-invasive Examination of Coronary Arteries by means of DSA with Synchrotron Radiation - II. In-vivo Investigations, DESY SR 86-10 (1986) (to be published in IEEE Computer Science).
/12/ K. Engelke: Ein oszillierender Monochromator für Koronarangiographie mit Synchrotronstrahlung, Diploma thesis (in German). University of Hamburg (1984).
/13/ W. Graeff, W.-R. Dix, K. Engelke, C.-C. Glüer, J. Heuer, H. Jabs, W. Kupper, K.-H. Stellmaschek: NIKOS - A System for Non-invasive Angiography with Synchrotron Radiation, Proc. CAR 87 (to be published).
/14/ W.-R. Dix, K. Engelke, C.-C. Glüer, W. Graeff, W. Kupper, K.-H. Stellmaschek: Image Processing for DSA in Energy Subtraction Mode, Proc. CAR 87 (to be published).
/15/ E. Rubenstein, R. Hofstadter, H.D. Zeman, A.C. Thompson, J.N. Otis, G.S. Brown, J.C. Giacomini, H.J. Gordon, R.S. Kernoff, D.C. Harrison, W. Thomlinson: Transvenous coronary angiography in humans using synchrotron radiation, Proc. Nat.Acad.Sci. USA 83 (1986) 9724.

/16/ SPIDER - Subroutine Package for Image Data Enhancement and Recognition, Handbook (1983)
/17/ J.Tobis, U.Nalcioglu, L.Isert, W.D.Johnston, W.Roeck, E.Castleman, B.Bauer, B.Montenelli, W.Henry: Detection and quantitation of coronary artery stenoses from DSA compared to 35-mm film cine angiograms, Am J Cardiol 56 (1984) 237.
/18/ W.K. Pratt: Digital Image Processing (1978) 311.
/19/ N.Yokoya, T.Kitahashi, K.Tanaka, T.Asano: Image segmentation scheme based on a concept of relative similarity, 4th International Joint Conference on Pattern Recognition (1978) 645.
/20/ M.Nagao, T.Matsuyama: Edge preserving smoothing, Computer Graphics and Image Processing, Vol.9, No.4 (1979) 394.
/21/ T.S.Huang, G.J.Yang, G.Y.Tang: A fast two-dimensional median filtering algorithm, 1978 IEEE Computer Society Conference on Pattern Recognition and Image Processing (1978) 128.
/22/ W.Frei, C.C.Chen: Fast boundary detection: A generalization and a new algorithm, IEEE Trans., C-26, No.10 (1977) 988.
/23/ R.Brennecke: A Bottelneck Model of Imaging Systems for Digital Angiocardiography, Proc. of Progress in Digital Angiocardiography (1986) (to be published).
/24/ K.Assmann, R.Venema, K.H.Höhne: The ISQL Language - A Software Tool for the Development of Pictorial Information Systems in Medicine, in S.-K. Chang et al. (eds.), Visual Languages, Plenum Press, New York (1986) 261.

Acknowledgement

We thank the Werner Otto Stiftung for financial support. We gratefully appreciate the encouraging support for this work from the DESY directors and from the management of HASYLAB. The support of the DESY computer center, the DESY workshops, the technical staff of HASYLAB, the Dept. of Veterinary Medicine, the Dept. of Pathology, and the Dept. of Computer Science in Medicine (IMDM) of the University Hospital Hamburg-Eppendorf is gratefully acknowledged. The authors would like to thank Miss L.Schlüter for assistance in preparing the dogs for the investigations and M.Riemer for assistance in using the image processing system of the IMDM. We thank L. Csepregi from the FHG-Institut für Mikrostrukturtechnik, Berlin, for the preparation of the thin Laue crystals.